# Martensitic transformation of a Ni-Al alloy. I. Experimental results and approximate structure of the seven-layered phase

Y. Noda*
*Faculty of Engineering Science, Osaka University, Toyonaka, Osaka 560, Japan*

S. M. Shapiro and G. Shirane
*Brookhaven National Laboratory, Upton, New York 11973*

Y. Yamada
*Institute for Solid State Physics, The University of Tokyo, Roppongi, Tokyo 106, Japan*

L. E. Tanner
*Lawrence Livermore National Laboratory, Livermore, California 94550*
(Received 26 April 1990)

Neutron-diffraction experiments were performed in order to investigate the structure of the thermoelastic martensite of the $Ni_{62.5}Al_{37.5}$ alloy. The following results were obtained: (i) the low-temperature phase has a seven-layered monoclinic unit cell (7*M* martensite). (ii) Anomalous shifts of the superlattice peaks from the commensurate position were observed, which could not be explained by an ordinary incommensurate structure. At the same time, anomalous broadenings of the peak profiles were also observed. The overall feature of the incommensurability and the broadening was tentatively understood by considering that there are two slightly different monoclinic lattices coexisting in the crystal. (iii) Ignoring these anomalous features, the approximate structure was investigated following three different procedures: (a) Analysis on the $(5,\bar{2})$ stacking-sequence model; (b) analysis on the pseudospin model; and (c) model-free analysis based on the postulated space group $P2/m$.

## I. INTRODUCTION

Martensitic transformations in alloys have been studied for nearly a century in view of the various important applications.[1] Recently, much attention has been focused on the shape memory effect exhibited by bcc-based alloys which undergo a thermoelastic martensitic transformation. The Ni-Al alloy is known to belong to this class of materials.

On the other hand, from an academic point of view, the martensitic (nondiffusional) phase transformation is understood in terms of the inherent lattice instability of the metallic bcc structure which manifests itself by the existence of low-lying transverse-acoustic phonons propagating along the [110] direction of the cubic lattice. The crystal structure in the low-temperature phase (thermoelastic martensite) is basically described by the "freezing" of a particular phonon accompanied by a macroscopic strain. That is, the static internal distortion of the lattice in the low-temperature phase corresponds to the displacement pattern of the relevant soft-phonon mode.

A typical example of the soft-phonon behavior was recently found in the $Ni_xAl_{1-x}$ alloy. In the concentration range of $0.60<x<0.64$, this alloy has a CsCl-type (ordered bcc) structure at room temperature and undergoes a martensitic transformation at low temperature.[2,3] Recent inelastic neutron-scattering experiments[4–7] by Shapiro *et al.* revealed that there exists a pronounced dip in the dispersion of the transverse-acoustic branch around $\mathbf{q}\sim\frac{1}{7}[110]_c$ accompanied by elastic diffuse scattering.[8] The elastic component seems to be related to the tweed pattern observed by electron microscope studies[2,9] in this alloy.

The structure of the martensite of the Ni-Al alloy was first studied by Martynov *et al.* for the $x=0.631$ alloy.[10] They performed an x-ray-diffraction experiment of a tensile martensite which was induced by the external tension at room temperature. The amount of deformation was a 4.5% elongation along the $[110]_c$ direction. From the observed x-ray-diffraction pattern, they concluded that the tensile martensite of the Ni-Al alloy has a monoclinic unit cell constructed by seven layers of $(110)_c$ atomic planes. Let us call the martensite with the seven-layered monoclinic unit cell "7*M* martensite" hereafter, instead of "7*R*" as is frequently used in the literature. Martynov *et al.* studied the structure of the 7*M* martensite based on their experimental results, and proposed a $(5,\bar{2})$ stacking sequence (using Zhdanov's notation)[11] of the $(110)_c$ planes. The periodicity of the proposed martensite structure having seven layers of $(110)_c$ planes is consistent with the observed "soft mode" with the wave vector $\mathbf{q}\sim\frac{1}{7}[110]_c$. However, the displacement of each layer to construct the $(5,\bar{2})$ stacking sequence is certainly not expressed by the "frozen" pattern of the harmonic phonon mode. Furthermore, the precise structure of the thermally induced martensite of the Ni-Al alloy is not yet estab-

 

lished.

The purpose of the present paper is to study the structure of the thermally induced $7M$ martensite precisely and to investigate the microscopic mechanism of the martensite transformation of this alloy. Preliminary results were already published elsewhere.[5-7,9,12]

## II. EXPERIMENT

Precise neutron-scattering experiments were performed at the High Flux Beam Reactor of the Brookhaven National Laboratory. The single crystals of $Ni_{62.5}Al_{37.5}$ were grown at the United Technology Research Center. The sample was cubic in shape ($5\times5\times5$ mm$^3$) and was heat treated to reduce compositional inhomogeneities. In order to mount it stress free, it was wrapped in Al foil and glued on an aluminum rod and then installed in a sealed aluminum container filled with He gas as the heat exchanger. The sample temperature was controlled by a Displex refrigerator. The transition temperature $T_M$ of this particular sample was determined to be approximately 80 K. The intensity data were collected at 15 K. Measurements were mainly performed on an $(HK0)_c$ zone of the cubic reciprocal lattice which became the $(H0L)_m$ zone in the monoclinic martensitic phase. The elastic neutron-scattering measurements were performed under the following conditions: for the high-resolution measurements a 30.4-meV incident energy ($\lambda=1.640$ Å) with a Ge(111) monochrometer and a PG(002) analyzer were utilized. Another experimental setting of 60-meV incident energy ($\lambda=1.168$ Å) with a PG(002) monochrometer and a PG(004) analyzer was used to collect the intensity data with higher $(H0L)_m$ indices.

The structure of the room-temperature phase ($\beta_2$ phase) is CsCl type with a lattice parameter of $a_0=2.858$ Å. When the sample was cooled down from room temperature, a domain structure appeared at $T_M$ due to transformation to the monoclinic lattice so that each Bragg reflection in the $\beta_2$ phase split into several spots. After careful survey of the splitting in the reciprocal space, we could classify each Bragg reflection as belonging to one of a few domains of the low-temperature monoclinic lattice.

Below $T_M$, we also observed superlattice reflections along the $\langle 110\rangle_c$ direction characterizing the $7M$ martensite structure. In Fig. 1, the reciprocal lattice of the martensite phase is shown schematically. The relative intensities of the observed superlattice peaks are also indicated by solid circles. The position of these peaks was almost, but not exactly, at $n/7(110)_c$ ($n$ is an integer). That is, the diffraction pattern apparently showed a so-called "incommensurability." Not only that, but the line shape of the peaks was anomalously broadened along the [110] direction. Some of them had a shoulder peak or even exhibited splitting into double peaks. The details of the anomalous peak shift and broadening will be discussed separately in Sec. IV.

We collected the intensity data up to $(40L)_m$ reflections by using a high-resolution setting of the spectrometer with 30.4-meV incident energy. The data on the $(50L)_m$ and $(60L)_m$ lines were added using 60-meV incident energy. The total number of observed data in the form of the structure factors $F_{ob}(H0L)$ was 136.[13]

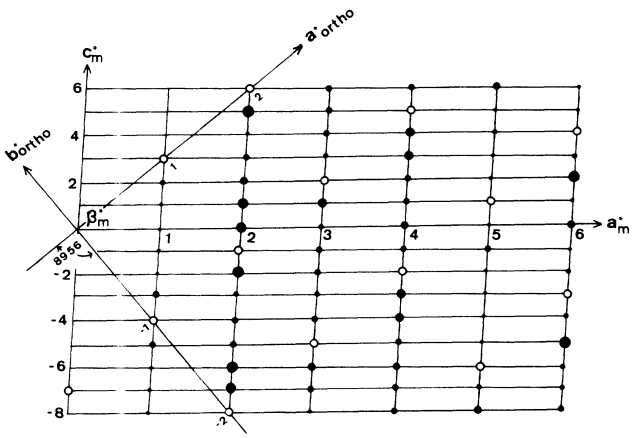


FIG. 1. Schematic diagram of the position and the intensity distribution of the superlattice reflections on the $(H0L)_m$ plane. The pseudo-orthorhombic axes corresponding to the original cubic reciprocal axes, $\mathbf{a}^*_{ortho}$ and $\mathbf{b}^*_{ortho}$ are also shown. The lattice given by $\mathbf{a}^*_m$ and $\mathbf{c}^*_m$ gives a monoclinic unit cell. The Bragg reflections corresponding to the original cubic lattice are marked by the open circles. The newly appeared superlattice Bragg reflections are given by the solid circles whose sizes represent, approximately, the relative intensity.

## III. APPROXIMATE STRUCTURE OF THE $7M$ PHASE

As is discussed in the preceding section, the peaks are not exactly at the commensurate positions and even tend to show splitting into double-peak structures. Because of this fact, we cannot define the monoclinic reciprocal lattice frame uniquely to describe all of the Bragg peak positions. In this section, we discuss the approximate structure by ignoring the anomalous "incommensurability;" that is, we assume the peaks at the exact $n/7$ positions. The lattice parameters were determined using $(206)_m$, $(020)_m$, and $(20\bar{8})_m$, which correspond to the original Bragg reflections $(200)_c$, $(00\bar{2})_c$, and $(0\bar{2}0)_c$, respectively. The unit cell of the $7M$ martensite is monoclinic as shown in Fig. 1 and the obtained lattice parameters at 15 K are

$$\begin{aligned} a_m &= 4.172 \text{ Å}, \\ b_m &= 2.690 \text{ Å}, \\ c_m &= 14.450 \text{ Å}, \\ \beta_m &= 94.37^\circ, \\ V_m &= 161.7 \text{ Å}^3. \end{aligned} \tag{1}$$

These values are in excellent agreement with those given by Martynov *et al.* for the stress-induced martensite of NiAl.[10] Therefore, the thermoelastic martensite phase and the tensile martensite phase of the Ni-Al alloy are considered to be identical. The relationship of the lattice frame between the parent cubic cell and the $7M$ martensite cell is given by

$$\mathbf{a}_m^* = (4\mathbf{a}_c^* - 3\mathbf{b}_c^*)/7 ,$$
$$\mathbf{b}_m^* = -\mathbf{c}_c^* , \quad (2)$$
$$\mathbf{c}_m^* = (\mathbf{a}_c^* + \mathbf{b}_c^*)/7 ,$$

in the reciprocal space. When the reciprocal cell is referred to the original cubic lattice with $a_c^* = 2.198$ Å$^{-1}$ at room temperature, the lattice is regarded to transform to a pseudo-orthorhombic lattice with $a_{\text{ortho}}^* = 2.072$ Å$^{-1}$, $b_{\text{ortho}}^* = 2.219$ Å$^{-1}$, $c_{\text{ortho}}^* = 2.336$ Å$^{-1}$, and $\gamma_{\text{ortho}}^* = 89.37°$ in the low-temperature phase (15 K), as shown in Fig. 1. In order to carry out the structure analysis, we followed three different procedures as described below.

*(1)* $(5,\bar{2})$ *stacking-sequence model.* The structure of the seven-layered martensite of the Ni-*Al* alloy was qualitatively analyzed by Martynov *et al.* based on a simple stacking-sequence model. As shown in Fig. 2, the $(110)_c$ plane of the CsCl-type structure is taken to be the rigid basal plane and the structure is defined by specifying the stacking sequence of the $(110)_c$ planes along the $[110]_c$ direction. Each $(110)_c$ plane shifts relative to the neighboring planes by $+\Delta u_0$ or $-\Delta u_0$. (See Fig. 2.) In order to specify the stacking sequence, it is convenient to use Zhdanov's notation,[11] which is conventionally used to define the $ABC\cdots$-type stacking sequence of the hexagonal-based long-period structures. Notice, however, that, in the case of ideal hexagonal layer stacking, $\Delta u_0$ is fixed to be $\Delta u_0 = \frac{1}{6}$. In the present case, where the lattice is monoclinic, $\Delta u_0$ is taken to be an adjustable parameter.

Martynov *et al.* analyzed their x-ray data and proposed $(5,\bar{2})$ stacking in the Zhdanov's notation with $\Delta u_0 = a_m/12$ (model *a* in Tables I and II). However, it is noticed that once the $(5,\bar{2})$ stacking is assumed, the proper value of the parameter $\Delta u_0$ should be experimentally given by the following equation:

$$c_m \sin(\beta_m - 90) + (5-2)\Delta u_0 = a_m/2 . \quad (3)$$

When the observed values in Eq. (1) are used, we find the value $\Delta u_0$ to be $a_m/12.71$. The structure with the above $\Delta u_0$ value may be considered an improved $(5,\bar{2})$ stacking model (model *b* in Tables I and II).

The positional parameter $x_j$ $(j = 1-6)$ of each atom in the monoclinic unit cell is readily calculated from the parameter $\Delta u_0$. For later convenience, we take the origin of the unit cell as shown in Fig. 3. Notice that the symmetry of the structure is described by the space group $P2/m$ with the center of inversion and the twofold axis at the origin of the unit cell. The coordinate $x_j$ of models *a* and *b* in this monoclinic unit cell is given in the model *a* and *b* columns of Table I and II.

In order to carry out the structure analysis, we calculated the structure factors based on the above models and compared them with the observed values $F_{\text{ob}}$. Since the positional parameters are all fixed, the adjustable parameters for the least-squares-fitting procedure are the scale factor and the anisotropic Debye-Waller factors $B_{ij}$. For

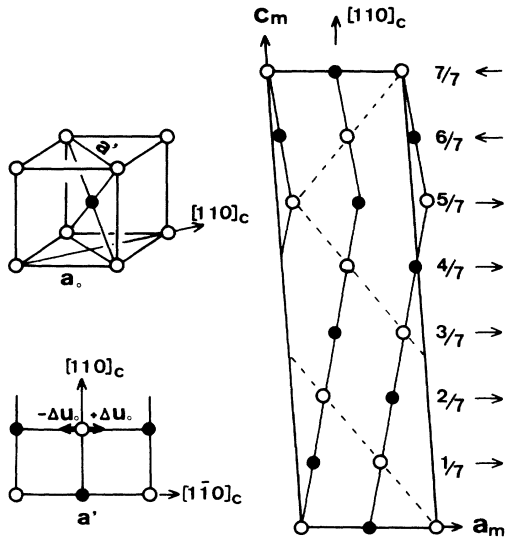


FIG. 2. The construction of the $(5,\bar{2})$ stacking sequence of $(110)_c$ planes. Each $(110)_c$ plane shifts relative to the neighboring planes in either plus or minus directions by $\Delta u_0$. The $(5,\bar{2})$ stacking means that five successive layers are shifted in the plus direction, followed by two successive layers shifted in the minus direction.

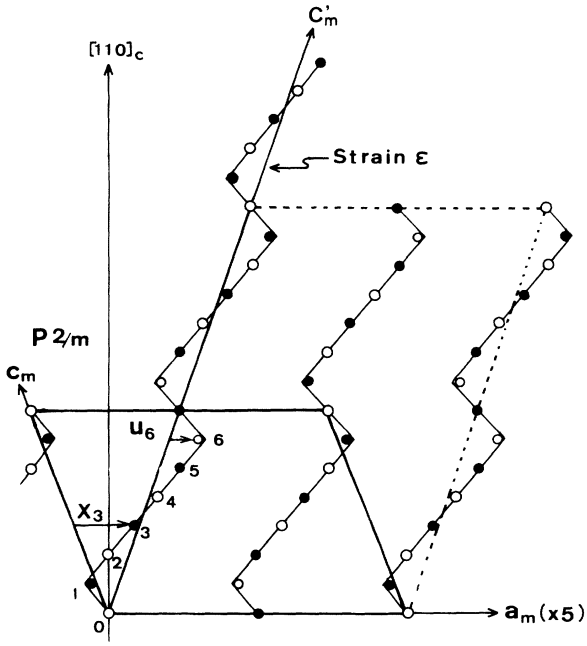


FIG. 3. The structure of the 7*M* martensite of the Ni-Al alloy belonging to the space group $P2/m$. The origin of the unit cell is shifted from Fig. 2 so that the center of inversion and the twofold axis are at the origin. For the clarity of the figure, the $a_m$ direction is expanded by five times. Independent positional parameters in the $P2/m$ unit cell are those for atoms $j = 1$, 2, and 3. The $x_3$ value is indicated by the arrow. The internal displacement $u_j$ is defined as the displacement from the original cubic $[110]_c$ line (the $c_m'$ line in the figure). Only $u_6$ is indicated in the figure. Notice the positions of the atoms $j = 1$ and 6 are appreciably off from the thin zigzag line which indicates the atomic positions of the $(5,\bar{2})$ stacking-sequence model. The slope of the $c_m'$ line corresponds to the bulk strain $\epsilon$.

TABLE I. Positional parameters for each model. (a) Martynov's $(5,\bar{2})$ stacking model. There are no adjustable positional parameters. (c) Pseudospin model. The values from $x_1$ to $x_6$ are fixed by the condition to form the embryonic mode. (d) Conventional structure analyses. The values from $x_1$ to $x_3$ are left as the adjustable parameters. The values from $x_4$ to $x_6$ are fixed by the condition to satisfy symmetry properties of the space group $P2/m$. The parameters of model $b$, which are not shown in the table explicitly, are given by defining the $x_1$ value in model $c$ as $x_1=-0.0410$.

| $j$ | | | $a$ | $c$ | $d$ |
|---|---|---|---|---|---|
| 0 | Al | $x_0$ | 0 | 0 | 0 |
| 1 | Ni | $x_1$ | $-\frac{2}{42}$ | $x_1$ | $x_1$ |
| 2 | Al | $x_2$ | $\frac{3}{42}$ | $0.6x_1+0.1$ | $x_2$ |
| 3 | Ni | $x_3$ | $\frac{8}{42}$ | $0.2x_1+0.2$ | $x_3$ |
| 4 | Al | $x_4$ | $\frac{13}{42}$ | $-0.2x_1+0.3$ | $1-(x_3+\frac{1}{2})$ |
| 5 | Ni | $x_5$ | $\frac{18}{42}$ | $-0.6x_1+0.4$ | $1-(x_2+\frac{1}{2})$ |
| 6 | Al | $x_6$ | $\frac{23}{42}$ | $-x_1+0.5$ | $1-(x_1+\frac{1}{2})$ |

simplicity, we assumed common Debye-Waller factors for all atoms, leaving only three adjustable $B$ factors: $B_{11}$, $B_{13}$, and $B_{33}$. As the scattering length of neutrons, we have used $b_{\mathrm{Ni}}=10.3\times10^{-13}$ cm for nickel-site atoms as given in the literature, while $b_{\mathrm{Al}}=5.7\times10^{-13}$ cm was used for effective aluminum atoms because the aluminum site is considered to be randomly substituted by the excess nickel atoms. In Table II, the obtained fitting parameters for models $a$ and $b$ are tabulated. The reliability factor ($R$ factor) of the structure analysis for model $a$ is $R=20.5\%$, which is significantly reduced to 16.7% for model $b$. The crucial difference between the models is manifested in that, in model $a$ (Martynov's model), an accidental extinction rule holds for the $(60L)_m$ reflections due to the choice of the specific value of $\Delta u_0(=a_m/12)$. In our neutron-scattering experiments, we observed weak but well-defined peaks on the $(60L)_m$ line.

*(2) Pseudospin model.* Recently, Fuchizaki *et al.*[14–16] proposed an alternative model to describe the martensite structures, in general, based on microscopic considerations. They specify a particular local vibrational mode of a cluster of atoms called the "embryonic" mode, which is eventually expressed by a pseudospin variable. By a statistical treatment of the pseudospin system, it has been shown that the martensite phase is characterized by the "ferro"-type ordered state of the pseudospins.

The atomic position in the ordered phase is given by[17]

$$\mathbf{r}_{lk}=(\mathbf{1}+\epsilon)\cdot\mathbf{r}_l^0+r_k^0+\xi\mathbf{e}_k^{\mathrm{emb}}\ , \tag{4}$$

where $\epsilon$ is the strain tensor, $\mathbf{r}_l^0$ is position vector of the $l$th unit cell, $\mathbf{r}_k^0$ is the position of the $k$th atom in the undistorted cubic lattice, $\mathbf{e}_k^{\mathrm{emb}}$ is the $k$th component of the normal coordinate of the embryonic mode, and $\xi$ is the amplitude of the mode. In the particular case of the $7M$ martensite, the embryonic mode is identified as the "tilting" motion of the atomic cluster composed of six successive $(110)_c$ planes [see Fig. 7(b) in Ref. 14], and $\mathbf{e}_k^{\mathrm{emb}}$ is given by

$$\begin{aligned}&\mathbf{e}_k^{\mathrm{emb}}\sqrt{2/35}(k-\tfrac{7}{2})\mathbf{e}_0\quad(k=1-6)\ ,\\&\mathbf{e}_0\|[110]\ .\end{aligned} \tag{5}$$

It should be pointed out that, in this pseudospin model, the amplitude of the embryonic mode $\xi$ or the tilting angle of the cluster is left as the unknown parameter to define the atomic positions from Eq. (4). Accordingly, in this model (model $c$) the fitting parameters to carry out the structure analysis have increased by one as compared with the cases of the previous models. The positional parameters of model $c$ are tabulated in the model $c$ column of Table I. The results of the least-squares fitting based on model $c$ are also given in the model $c$ column of Table II. The $R$ factor is 15.8%, marginally better than model $b$.

*(3) Model-free structure analysis.* As the most general treatment, we follow the conventional procedure of the structure analysis. That is, the structure factor associated with the postulated space group is directly compared with the values of $F_{\mathrm{ob}}$ by adjusting the unknown positional parameters allowed for the space group (model $d$ in Tables I and II). The postulated space group in the present case is $P2/m$ and the unknown positional parameters are $x_1$, $x_2$, and $x_3$ as given in Fig. 3. All of the atomic positions in the unit cell are generated by the symmetry operation of $P2/m$ from these positional parameters if we assume that the basal plane is kept rigid, and whence there is no internal displacement within the basal plane. The results of the least-squares fitting are given in

TABLE II. Obtained fitting parameters for each model. The numerical values in the parentheses indicate that these values are not the fitting parameters but are either the fixed values or deduced from the fitted parameters for each model. The estimated error of each parameter is given at the last digit in parentheses.

| | $a$ | $b$ | $c$ | $d$ |
|---|---|---|---|---|
| $x_1$ | (−0.0476) | (−0.0410) | −0.0371(5) | −0.0343(7) |
| $x_2$ | (0.0714) | (0.0754) | (0.0777) | 0.0731(6) |
| $x_3$ | (0.1905) | (0.1918) | (0.1926) | 0.1921(1) |
| $B_{11}$ | 0.0376(1) | 0.0364(3) | 0.0365(1) | 0.0364(3) |
| $B_{13}$ | 0.0003(1) | 0.0003(1) | 0.0003(1) | 0.0003(1) |
| $B_{33}$ | 0.0019(1) | 0.0019(1) | 0.0019(1) | 0.0019(1) |
| $R$ (%) | 20.5 | 16.7 | 15.8 | 14.1 |

the model $d$ column of Table II. The $R$ factor drops to 14.1%.

Let us consider the physical implication of the obtained parameters $x_j$ in model $d$ in comparison with the simple stacking-sequence model (model $b$). As shown in Table II, the $|x_1|$ value of model $d$ is significantly smaller than that of model $b$, while the differences tend to become marginal for $x_2$ and $x_3$. Physically, this means that the zigzag atomic chains in the ideal $(5,\bar{2})$ stacking as given in Fig. 3 tend to be rounded at the corners so that the zigzag chains become smoother than the simple stacking sequence.

In order to make this point clear, let us perform a Fourier analysis of the displacement field. We express the obtained structural parameters $x_j$ by the sum of the internal displacement $u_j$ referred to the undistorted atomic position of the original cubic lattice and the displacement due to the external strain $\epsilon$ as shown in Fig. 3. It should be emphasized that the meaning of the displacement $u_j$ is different from the parameter $\Delta u_0$ which is defined by the relative shift between the neighboring layers. The relationship between the parameters $x_j$ and the internal displacement $u_j$ is

$$x_j = u_j/a_m + j/14 , \tag{6}$$

where the second term in Eq. (6) gives the strain component as is more explicitly expressed in Eq. (4). Since the superlattice reflections appear at $\pm n/7(110)_c$ ($n$ is an integer), the relevant Fourier components (modulation waves) have the wave vector $q=\frac{1}{7}$ and its higher-order components. The internal displacement is expressed by the Fourier series as

$$u_j = \sum_{n=1}^{3} A_n \sin(2\pi \cdot n/7 \cdot j) , \tag{7}$$

where $A_n$ is the amplitude of the modulation wave. We introduced only sine terms in the Fourier analysis in Eq. (7) because of the inversion symmetry in space group $P2/m$. It is worthwhile to compare this fact with the recent theoretical argument by Gooding and Krumhansl[18] in which two independent modulation waves with $q=\frac{1}{7}$ and $\frac{2}{7}$ were introduced for the free-energy expressions. From Eqs. (6) and (7), we find the $A_n$ amplitudes uniquely. The results are tabulated in Table III. From the obtained amplitudes, we see that the displacement field tends to be more sinusoidal as compared with the simple $(5,\bar{2})$ stacking sequence by reducing the higher-order modulation components. Nevertheless, the magnitude of the higher-order components are still not negligible in our final structure analysis (model $d$), which indicates that the modulation wave is highly anharmonic and the displacement might be preferably expressed by the local embryonic mode discussed in the pseudospin model.

TABLE III. The amplitudes of the Fourier components for the displacement waves in models $b$ and $d$ in angstroms. The ratio relative to the amplitude of the fundamental wave is also given in the table.

| | Model $b$ | Ratio | Model $d$ | Ratio |
|---|---|---|---|---|
| $A_1$ | −0.3896 | 100 | −0.3822(28) | 100 |
| $A_2$ | −0.1496 | 38 | −0.1321(8) | 35 |
| $A_3$ | −0.0427 | 11 | −0.0307(2) | 8 |

## IV. ANOMALOUS PEAK SHIFT AND PEAK BROADENING

In the course of the analysis of the approximate structure of the $7M$ martensite phase described above, we have ignored the anomalous peak shift and peak broadening of the satellites. In this section, we summarize the features of shifts and broadenings of the peaks and discuss the systematic behaviors in these quantities which indicate that these anomalies are intrinsic effects.

In Fig. 4, the intensity profile of the neutron scattering scanned along the $[40L]_m$ direction is shown as a typical example of the observed spectra. As is clearly shown in the figure, the peak position of each satellite reflection deviates from the exact commensurate position of the monoclinic reciprocal lattice. Such a shift is commonly observed in the diffraction pattern from an incommensurate structure. However, it is found that the amount of the shift of each reflection does not specify a single wave vector of the incommensurate wave, indicating that this phase is not described in terms of an ordinary incommensurate structure. Moreover, each profile shows either shoulder or asymmetric tailing as is seen in the inset of Fig. 4. Some of the peaks even exhibit splitting to give a double-peak structure. In order to show the features of the anomalous "incommensurability," the peak shift $\Delta$, defined by $(H0L+\Delta)_m$, is plotted as a function of the index $L_m$ for each $H_m$ value. (See Fig. 5.) The solid circles in the figure denote the reflections which correspond to the original cubic Bragg reflections. For instance, the $(206)_m$ and $(20\bar{8})_m$ Bragg points correspond to $(200)_c$ and $(0\bar{2}0)_c$, respectively. When a profile shows either splitting or a clear shoulder peak, we choose the peak position of the major peak. The subsidiary peak positions

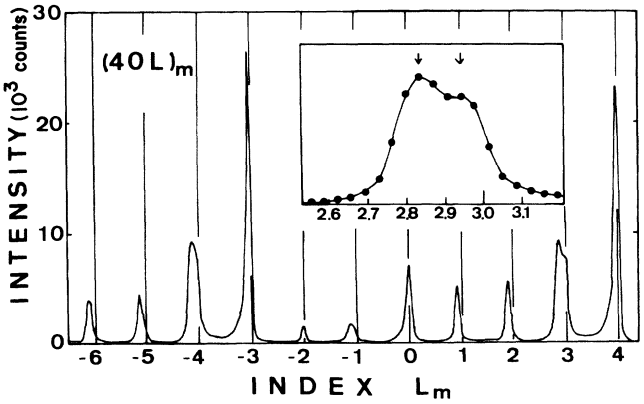


FIG. 4. Intensity profile along the $[40L]_m$ direction observed by the high-resolution setting. The straight lines give the exact (commensurate) positions of the monoclinic lattice. The inset shows the $(403)_m$ peak expanded along the $L_m$ line to demonstrate the shoulder peak behavior more clearly.

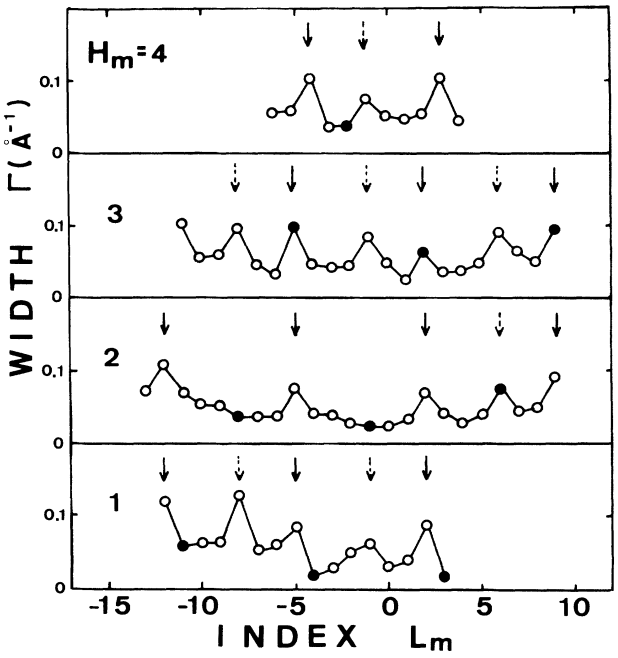


FIG. 5. The diagram of the peak shift $\Delta$ $(H_m 0 L_m)$ from the commensurate positions as a function of $L_m$ and $H_m$. The circles denote the peak position of the major peaks, while the triangles denote those of the minor peaks or of the clearly separable peak in the spectra. The solid circles (triangles) indicate the reflections corresponding to the original cubic lattice.

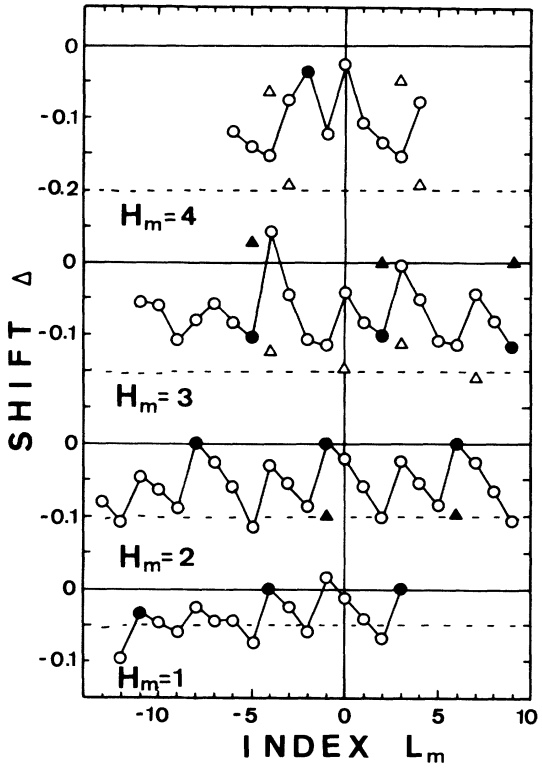


FIG. 6. The diagram of the width $\Gamma$ of each spectrum as a function of $L_m$ and $H_m$. The width due to the instrumental resolution is already subtracted. The positions of extraordinarily large $\Gamma$ are indicated by the solid or the dashed arrows showing the periodicity of $L_m = 7$.

are also indicated in the diagram by triangles. Notice that, if the lattice is perfectly commensurate, all points should be on the $\Delta = 0$ lines. We also plotted the width of the profile as a function of index $L_m$ (Fig. 6). The width $\Gamma$ is defined by the full width at half maximum of the peak intensity so that the spectra having a double-peak structure or a shoulder peak have a significantly larger $\Gamma$ value as indicated by arrows in the figure.

From Figs. 5 and 6, we immediately notice that there exists a periodic behavior both in $\Delta$ and $\Gamma$ along the $L_m$ direction. In particular, the period of seven is clearly seen in the diagram of $\Delta$. The physical origin of this periodicity will be discussed in the forthcoming paper (paper II of this series of papers).

We also notice another important systematic behavior, that the average peak shift $|\bar{\Delta}|$ of each $[H0L]_m$ line increases with increasing $H_m$. The overall feature of this systematic behavior of $|\bar{\Delta}|$ becomes understandable by considering two monoclinic lattices with different monoclinic angles:[19–24] $\beta_m^{(1)} = 94.37°$ and $\beta_m^{(2)} = 93.82°$. The former, which has already been defined in the previous section, is determined by using the major Bragg peaks $(206)_m$ and $(20\bar{8})_m$. The latter is determined using the subsidiary peak positions indicated by triangles in Fig. 5. While the peak positions for the lattice commensurate with $\beta_m^{(1)}$ are on the $\Delta = 0$ lines, those for $\beta_m^{(2)}$ are expected to be on the dashed lines given in Fig. 5. Notice that the separation between the pairs of the solid and dashed lines increases linearly with $H_m$.

Since the observed satellite points are "oscillating" between each pair of the solid and dashed lines, the simplest interpretation of the shift diagram would be that there are, in fact, two monoclinic lattices with different monoclinic angles,

$$\beta_m^{(1)} = 94.37° , \quad \beta_m^{(2)} = 93.82° , \tag{8}$$

coexisting in the crystal.[25] Such a two-monoclinic mixed state seems to be similar to the recently observed two-tetragonal mixed state[26–28] in FePd and may also be interpreted in terms of the theoretically proposed crest-riding-periodon state.[29–31]

While the assumption of coexistence of the two monoclinic lattices gives a plausible explanation of the overall behavior of $|\bar{\Delta}|$, it is still far from explaining the subtle shift diagram of the individual reflections $\Delta$ as a function of $(H0L)_m$. The details of the physical interpretation of the shift diagram itself will be given in paper II of this series of paper.

## V. SUMMARY

Neutron-scattering experiments were performed in order to investigate the structural aspect of the martensitic phase of the Ni-Al alloy. Below the martensitic transition temperature $T_M$, superlattice reflections at $n/7(110)_c$ ($n$ is an integer) were observed. It was con-

cluded that the thermoelastic martensite of the $Ni_{62.5}Al_{37.5}$ alloy has a seven-layered monoclinic cell (7*M* martensite) which is identical to the tensile martensite studied by Martynov *et al.*

Detailed observation of the satellite reflections in the monoclinic phase has revealed that the peak profile shows anomalous incommensurability and broadening along the $[110]_c$ direction. The peak shift $\Delta$ and the width $\Gamma$ show systematic behaviors when plotted against $L_m$, indicating that these effects are of intrinsic origin. The overall feature of the peak shift is understood by considering that there are two lattices with slightly different monoclinic angles coexisting, which is tentatively called a two-monoclinic mixed state. In this paper, we only investigated the approximate structure of the 7*M* martensite ignoring the anomalous shifts and broadenings of the observed spectrum.

Three different procedures were undertaken to carry out the structure analysis.

(1) Analysis based on the stacking-sequence model. The structure is defined by specifying the stacking sequence of the $(110)_c$ planes. The relative shift $\Delta u_0$ between the two successive $(110)_c$ planes is the structural parameter. The $(5,\bar{2})$ stacking model proposed by Martynov *et al.* belongs to this class. The *R* factor based on this (improved stacking-sequence) model is $R=16.7\%$.

(2) Analysis based on the pseudospin model. The structure is defined by the ferro-type ordered state of the pseudospin, which stands for the local tilted cluster of atoms. The tilt angle of the cluster is the structural parameter. The *R* factor based on this model is $R=15.8\%$.

(3) Model-free structure analysis. The conventional structure analysis was carried out where three positional parameters allowed for the space group $P2/m$ were adjusted. The final *R* factor is $R=14.1\%$.

The displacement pattern given by the model-free structure is Fourier analyzed and compared with the case of the $(5,\bar{2})$ stacking-sequence model. It was found that the simple stacking-sequence model overestimates the contribution of the higher harmonics in the context that the displacement pattern based on the model-free calculation tends to be more sinusoidal as compared with the zigzag configuration in the $(5,\bar{2})$ stacking sequence. Further discussions concerning transformation mechanisms, in particular, associated with the shift pattern, will be given in paper II of this series.

## ACKNOWLEDGMENTS

The authors would like to express their sincere thanks to Dr. K. Fuchizaki of Osaka University for many fruitful discussions. This work was supported by U.S.–Japan cooperative Neutron Scattering Program. One author (Y.N.) will also acknowledge the Yamada Science Foundation for financial support. All experiments were performed under the auspices of the U.S. Department of Energy (DOE) by the Brookhaven National Laboratory under Contract No. DE-AC02-76CH0016 and by Lawrence Livermore National Laboratory under Contract No. W-7405-ENG-48.

---

*Present address: Faculty of Science, Chiba University, Yayoi, Chiba 260, Japan.

[1]Z. Nishiyama, in *Martensitic Transformation*, edited by M. E. Fine, M. Meshii, and C. M. Wayman (Academic, New York, 1978).

[2]S. Chakravorty and C. M. Wayman, Metall. Trans. **7A**, 555 (1976).

[3]K. Enami, S. Nenno, and K. Shimizu, Trans. Jpn. Inst. Met. **14**, 161 (1973).

[4]S. M. Shapiro, J. Z. Larese, Y. Noda, S. C. Moss, and L. E. Tanner, Phys. Rev. Lett. **57**, 3199 (1986).

[5]S. M. Shapiro, B. X. Yang, G. Shirane, Y. Noda, and L. E. Tanner, Phys. Rev. Lett. **62**, 1298 (1989).

[6]S. M. Shapiro, B. X. Yang, G. Shirane, J. Z. Larese, L. E. Tanner, and S. C. Moss, Physica **156&157**, 59 (1989).

[7]G. Shirane, *Proceedings of the MRS International Meeting on Advanced Materials* (Material Research Society, Pittsburgh, 1989), Vol. 9, p. 3; S. M. Shapiro, Materials Science Forum **56-58**, 33 (1990).

[8]The soft phonon in the Ni-Al alloys is not exactly at $\mathbf{q}=\frac{1}{7}$ but rather the position in $\mathbf{q}$ space has concentration dependence (Ref. 4). For the sample of $Ni_{62.5}Al_{37.5}$, the phonon dispersion curve showed a marked, but incomplete, softening at $\mathbf{q}\sim\frac{1}{6}$ instead of $\mathbf{q}=\frac{1}{7}$ (Ref. 6).

[9]D. Schryvers, L. E. Tanner, and S. M. Shapiro, *Proceedings of the MRS International Meeting on Advanced Materials* (Material Research Society, Pittsburgh, 1989), Vol. 9, p. 35.

[10]V. Y. Martynov, K. Enami, L. G. Khandros, S. Nenno, and A. V. Tkachenko, Phys. Met. Metallogr. (USSR) **55**, 136 (1983).

[11]G. S. Zhdanov, Dokl. Akad. Nauk USSR **48**, 39 (1945). Also see, Z. Nishiyama, *Martensitic Transformation*, Ref. 1.

[12]Y. Noda, S. M. Shapiro, G. Shirane, Y. Yamada, K. Fuchizaki, and L. E. Tanner, Materials Science Forum **56-58**, 299 (1990).

[13]A table of numerical values of $F_{ob}(H0L)$ is available from the author.

[14]K. Fuchizaki, Y. Noda, and Y. Yamada, Phys. Rev. B **39**, 9260 (1989).

[15]K. Fuchizaki and Y. Yamada, Phys. Rev. B **40**, 4740 (1989).

[16]Y. Yamada, K. Fuchizaki, and Y. Noda, Materials Science Forum **56-58**, 107 (1990).

[17]Detailed discussions will be given in paper II of this series of papers, Y. Yamada, Y. Noda, and K. Fuchizaki, following paper, Phys. Rev. B **42**, 10 405 (1990).

[18]R. Gooding and J. A. Krumhansl, Phys. Rev. B **39**, 1535 (1989).

[19]This feature is somewhat reminiscent of the anomalous incommensurability observed in NiTi (Ref. 20) and AuCd (Ref. 21), whose origin has been extensively discussed (Refs. 15 and 22–24) in terms of the MLR or ghost lattice concept. However, the anomaly in NiAl is substantially different from the NiTi case in that all of the reflections including fundamental Bragg reflections suffer appreciable shift, while in NiTi only

the satellites exhibit incommensurability.

[20]S. M. Shapiro, Y. Noda, Y. Fujii, and Y. Yamada, Phys. Rev. B **30**, 4314 (1984).

[21]Y. Noda, M. Takimoto, T. Nakagawa, and Y. Yamada, Metall. Trans. **19A**, 265 (1988).

[22]M. B. Salamon, M. E. Meichle, and C. M. Wayman, Phys. Rev. B **31**, 7306 (1985).

[23]Y. Yamada, Metall. Trans. **19A**, 777 (1988).

[24]I. Folkins and M. B. Walker, Phys. Rev. B **40**, 255 (1989).

[25]This state is a "two-monoclinic mixed state" and definitely different from the ordinary microtwin structure because the two different observed regions have different monoclinic angles while variants in a twin structure must have the same monoclinic angle. Furthermore, the internal structures of the two different regions might be different from each other as discussed in Ref. 17.

[26]H. Seto, Y. Noda, and Y. Yamada, J. Phys. Soc. Jpn. **57**, 3668 (1988).

[27]H. Seto, Y. Noda, and Y. Yamada, J. Phys. Soc. Jpn. **59**, 965 (1990).

[28]H. Seto, Y. Noda, and Y. Yamada, J. Phys. Soc. Jpn. **59**, 978 (1990).

[29]G. R. Barsch, J. A. Krumhansl, L. E. Tanner, and M. Wuttig, Scr. Metall. **21**, 1257 (1987).

[30]G. R. Barsch and J. A. Krumhansl, Metall. Trans. **19A**, 761 (1988)

[31]F. Falk, Z. Phys. B **51**, 177 (1983).